Edinburgh Research Explorer

A numerical method for the design of ships with wind-assisted propulsion

A numerical method for the design of ships with wind-assisted propulsion

Ignazio Maria Viola[a,*], Matthieu Sacher[b], Jinsong Xu[c], Fei Wang[c]

[a]*Institute for Energy Systems, School of Engineering, the University of Edinburgh*
[b]*Ecole Superieure des Techniques Aeronautique et de Construction Automobile*
[c]*State Key Laboratory of Ocean Engineering, Shanghai Jiao Tong University*

Abstract

The present paper presents a numerical investigation on the potential of wind-assisted propulsion for merchant ships. In particular, a KVLCC2M hull was equipped with a set of wingsails inspired from those used in the 34th America's Cup. The combined thrust due to the propeller and the wingsails required to achieve a given cruising speed was computed by solving the equations of motion. For every wind direction, the wingsail trim was optimised with a genetic algorithm in order to minimise the thrust of the propeller. The aerodynamic forces and moments due to the hull and the wingsails were computed with Reynolds-averaged Navier-Stokes simulations, while the hydrodynamic forces on the hull and rudder were computed by adapting formulations developed for manoeuvrability applications. It was found that the aerodynamic efficiency of the wingsails is critical in order to gain a meaningful thrust contribution. The propeller thrust was decreased by about 10% when sailing crosswind, and the maximum benefit was achieved by sailing at low speed in strong wind conditions. The oil saving was found to be particularly sensitive to the wingsail aspect ratio, suggesting that an efficient wingsail should employ several tall wingsails rather than a few short and larger wingsails.

Keywords: Wind-assisted propulsion, Windships, Velocity Prediction Program, Wingsails, Sailing Yachts, Sustainable transport

*Corresponding author.
  Email address:* `i.m.viola@ed.ac.uk` (Ignazio Maria Viola)
  URL: `www.research.ed.ac.uk/portal/iviola/` (Ignazio Maria Viola)

1. Introduction

1.1. Wind Assisted Propulsion

In the 1980, oil price suddenly increased significantly and this led to the exploration of potential alternative propulsion systems that took advantage of the possibilities of sail technology. The research effort that was undertaken at that time towards wind-assisted propulsors is shown by several contributions that were presented at the International Symposium on Windship Technology (Satchwell, 1985). After several months the oil price dropped again and from 1980 to 1998 the continuous decrease of oil prices made conventional engines affordable again and developments in wind technology were abandoned. Oil prices started increasing again in 1998 and, since then, it has shown an almost constantly increasing upward trend. Today, the nominal price of oil has already doubled from the price peak in 1980. All experts agree that oil prices will continue to increase at least for the next ten years. The dependency on oil cost leads to the constant increase of the shipping cost for the approximately 90% of the goods that are traded in the world and shipped by sea. In trying to reduce their oil consumption, since 2008 many ships have reduced their cruising speed from 25 to 20 knots. A 20% speed reduction allows for a saving of about 40% in fuel consumption. With oil prices continuing to increase, many major companies have recently reduced the speed further to 12 knots. However, speed reduction is in conflict with the necessity of delivering the goods in a timely fashion to meet market demands and as such cannot decrease significantly further when the oil price increases. Therefore, wind power, which has been proven to be able to provide efficient auxiliary propulsion, is becoming attractive again.

On top of the need to uncouple shipping cost from oil price, there is a convincing environmental argument suggesting that the use of wind power must increase. The worldwide merchant fleet produces more than 3% of the total global carbon emissions (International Maritime Organisation, 2009). This merchant fleet emission is as much as the entire output of Japan, which is the 5th highest producer of carbon emissions (United Nations Statistics Division website, visited Sep 2011). These emissions have increased exponentially since the middle of the last century and may rise by a further 30% by 2020 (International Maritime Organisation, 2009). A significant and sudden reduction of these emissions is clearly urgently needed and existing sustainable technologies must be broadly used while new long-term highly innovative solutions are developed.

In order to quickly motivate the market towards using greener propulsors, legislation will bring about increasing taxes on carbon emissions. In the next few years, with oil price increases and the necessity of decreasing carbon emissions, the usage of sail technology is likely to increase fairly.

1.2. Potential Savings and Impact

The amount of fuel oil that can be saved using wind technology is widely debated. In 1986, a cargo wind-ship with rigid wing sails was built and she generated an average annual saving of between 15% and 30% of the previously consumed fuel rate (Cross, 1986). In 2000, a product carrier with rigid wing sails was designed for the Danish Ministry of Environment and Energy and she was estimated to enable an annual saving up to 15% of fuel (Rosander and Block, 2000). In 2007, full-scale tests showed that kites used together with conventional engines could enable an annual saving of up to 35% (Skysail website, visited July 2011). Although the use of kites has an interesting potential, the wide air space necessary to fly the kites efficiently and the difficulties in launching and landing the kites make this technology rather less attractive than sail technology. More recently, B9, the largest independent operator of wind-farms across the UK and Ireland with 49 sites and 750 turbines under its management, estimated that flexible sails fitted to ships could supply 100% of their thrust for 60% of the time (B9 Energy website, visited July 2011). These various numbers show that sail technology can be used to different operational extents. Also, the consideration of reduced average cruising speeds, allows sails to be more efficient and, at the same time, the reduced speed increases the ratio of the wind thrust over the thrust that is generated by the conventional engines.

Ocean-going low-speed bulk carriers and oil tankers can particularly benefit from wind-assisted propulsion. These ships can accommodate additional superstructures on deck. The low-speed operation increases the spectrum of wind directions where sails and wing sails can generate useful thrust. The long distances covered decreases the percentage of overall voyage time that is spent in restricted waters where sail-power might affect the freedom for manoeuvrability. There are 11000 bulkers and 8000 tankers of 5000 DWT (Dead Weight Tonnage) or greater that are operating worldwide and these two ship types together represent about 75% of the global ocean-going fleet in DWT (Lemper, 2011).

1.3. Velocity Prediction Program

The use of wind-assisted propulsion increases the complexity of the design process because many design parameters are strongly coupled. For instance, a sail area increase leads the thrust force to increase but also the side force, the yaw moment and the heel moment to increase, therefore also the resistance increases. Because both the thrust and the resistance increase, it is not trivial to compute whether a larger sail area is beneficial. A common approach in high-performance sailing yachts is to solve the coupled equations of motion with the aid of a computer program, namely Velocity Prediction Program (VPP). The first VPP was developed in 1970s to predict the performance of different sailing yachts in order to identify a handicap system for yacht races (Kerwin, 1978). Today VPPs are essential design tools to compare different candidate design solutions, for instance see Larsson (1990). Based on computation fluid dynamics (CFD), experimental fluid dynamics (EFD) or analytical formulations (AFD), models of how the aerodynamic and the hydrodynamic forces and moments vary with the key design parameters are used to solve all, or some, of the six equations of motion of the yacht (surge, sway, heave, roll, pitch and yaw). Most of the VPPs solve the surge, sway and roll equation.

On ships with wind-assisted propulsion, VPPs have been implemented (Rosander and Block, 2000; Ouchi et al., 2013) solving the yaw equation instead of the roll equation. This allows the significant effect of the rudder to be taken into account, while the maximum heel angle of ships is smaller than on sailing yachts and thus the heel equation can be uncoupled from the other equations of motion. In particular, Rosander and Block (2000) adopted a VPP developed by the Danish Meteorological Institute for the Modern Windship (Fig. 1a), while Ouchi et al. (2013) developed a VPP to design the Wind Challenger (Fig. 1b). Unfortunately, the algorithms implemented by these previous authors have not been published. In the present paper a VPP solving the surge, sway and yaw equations is presented, including the description of the flow and the models based on CFD and AFD.

In order to compute the sail forces, 3D models of the sails are typically tested with EFD or CFD, for instance in Fujiwara et al. (2003) and Altosole et al. (2014). Conversely, in the present approach, horizontal 2D wing sections are modelled with CFD and the computed aerodynamic coefficients are integrated along the span to estimate the total wingsail forces. The novelty of the proposed study is also how the boundary conditions are set for the
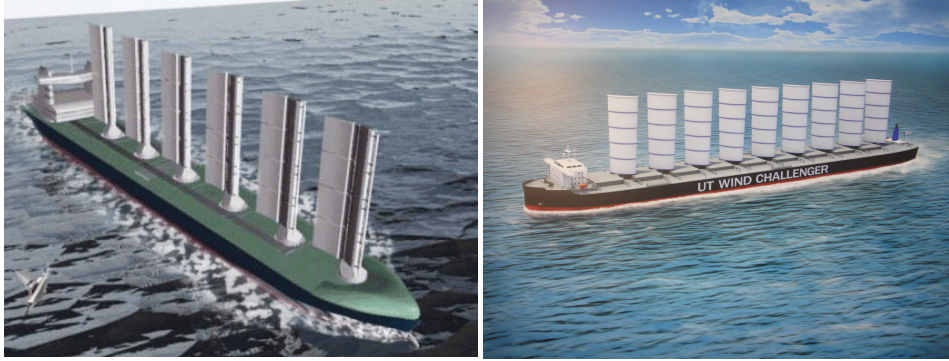
(a) The Modern Windship.   (b) The UT Wind Challenger.

Figure 1: Example of ships with wind-assisted propulsion.

CFD simulations and how the computed aerodynamic coefficients are scaled based on the apparent velocity wind profiles.

The rest of the paper is organised as Method (Sec. 2), Results (Sec. 3) and Conclusions (Sec. 4). The Method includes the description of ship and wingsail geometry (Sec. 2.1); the VPP algorithm (Sec. 2.2); the hydrodynamic models of the hull (Sec. 2.3) and rudder (Sec. 2.4); the aerodynamic models of the wind (Sec. 2.5), topsides (Sec. 2.6) and wingsails (Sec. 2.7). The results include the potential oil saving for different wind conditions (Sec. 3.1); ship speeds (Sec. 3.2); wingsail areas (Sec. 3.3) and wingsail aspect ratios (Sec. 3.4).

2. Method

2.1. Geometry

One of the limitations of the previous works (Rosander and Block, 2000; Ouchi et al., 2013) is that low efficiency rectangular curved plates were used for wind propulsion. In the present work, sails are inspired by the state-of-the-art technology used in the most recent America's Cup (Competitors of the America's Cup, 2012). Multi-element rigid wingsails are used and it is assumed that more than one wingsail can be installed on the deck (Fig. 2). These wingsails can generate much higher lift and lift/drag ratios than curved plates.

5

Figure 2: Artist's impression of the proposed windship.

The wingsail section was made of two airfoils in series with a small gap in between (Fig. 3). The sections of the foils, the gap between the foils, and the centre of rotation of the aft foil with respect to the aft foil, were chosen based on a preliminary investigation on wingsail optimisation for America's Cup wingsail catamarans (Sacher, 2013). The study was performed in collaboration with Owen Clark Design, a firm renown in high-performance yacht design. The fore foil was a NACA0012, the aft foil was a NACA0010, the fore foil chord was 6% longer than the aft foil chord. Such a thick fore foil (12% of the chord) and high-modulus carbon fibre are used in the America's Cup to achieve high cross-sectional strength and low weight. The low weight requirement is likely to be less important for a cargo ship than an America's Cup boat but, on the other hand, it is likely that wingsail will be made of steel, which have a lower modulus of elasticity than carbon fibre, and that a higher factor of safety will be adopted. Therefore a thick fore foil was adopted in this study as well. The gap between the foils when these were aligned was 2% of the aft foil. The aft foil can rotate around a pivoting point which was on the fore foil chord at 90% of the chord from the leading edge. The lateral plane of the wingsail was 260 m^2 and it was 38 m high.
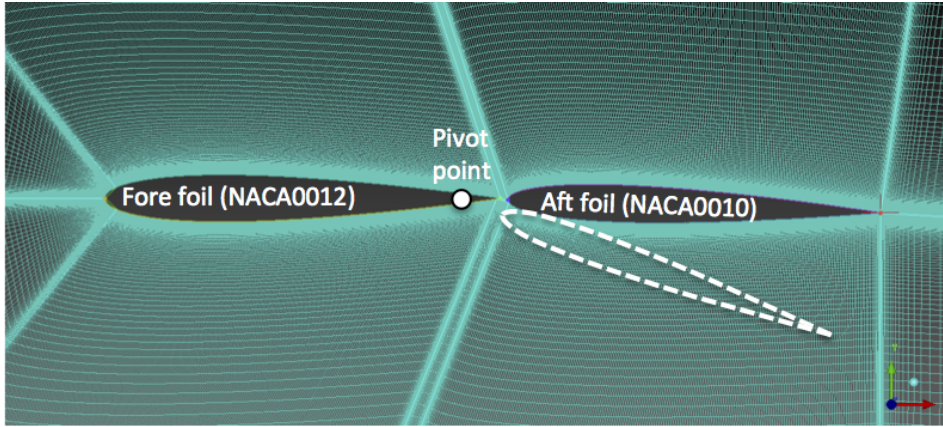
6

Figure 3: A horizontal section of the wingsail and the computational grid.

The KVLCC2M hull form was chosen as an example of a generic tanker. Her geometry can be downloaded from the webpage of the National Maritime Research Institute of Japan (National Maritime Research Institute of Japan website, visited in March 2014). A simplified pilothouse, a realistic rudder and a propeller were added. The key dimensions are summarised in Fig. 4 and Tables 1-3. The resistance coefficient with zero leeway angle was computed as suggested by Holtrop and Mennen (1982).
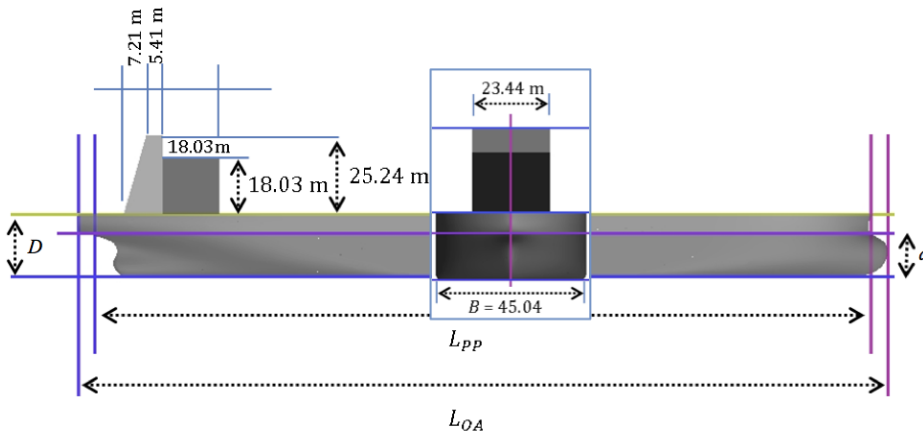

Figure 4: Rendering of the KVLCC2M hull form with a simplified pilothouse.

Table 1: Hull dimensions.

Length overall	L_{OA}	259.10	m
Length between perpendicular	L_{PP}	248.50	m
Depth	D	20.20	m
Breadth	B	45.05	m
Draft	d	16.15	m
Wetted surface area	S_{wet}	16475	m^2
Block coefficient	C_b	0.8099	-
Load waterline coefficient	C_w	0.9024	-
Midship section coefficient	C_m	0.9979	-
Resistance coefficient	C_t	0.004190	-

Table 2: Rudder dimensions.

Area	101.61	m^2
Height	13.62	m
Breadth	7.46	m

Table 3: Propeller dimensions.

Number of blades	4	-
Pitch	7.11	m
Diameter	9.86	m
Revolution	38.33	RPM
Area ratio	0.43	-

The wingsails generate significant lift and, depending on the wind direction, this can result in high side force. The aerodynamic side force must be balanced by a hydrodynamic side force, which is generated by the hull when sailing at a leeway angle. Unfortunately sailing with a leeway angle leads to a significant hull resistance increase. Alternatively, fin keels could be used to generate hydrodynamic side force. In particular, if the angle of attack of the fin keels was controllable, then the ship could sail with zero leeway angle in any condition. Therefore, if compatible with the ship operations, i.e. if the draft could be significantly increased, then high-aspect-ratio fin keels should be employed. The use of fin keels can also be used to balance the yaw

8

moments of the wingsails and the rudder. While modelling the fin keels in the VPP is simple and similar to the rudder, in the present work these were not modelled and the side force is generated by the hull sailing at a leeway angle.

2.2. Equations of motion and Optimisation

The reference system used is centred at the intersection of the ship mid-section, the ship symmetry plane and the water plane. The x axis points forward, the y axis points port and the z axis points upward. Symbols X and Y are used for forces in the x direction (surge) and y direction (sway), respectively, while N is used for the moment around the z axis (yaw). The equations of motion for a ship travelling with a constant forward velocity and zero angular velocity are as follows:

$$\sum X = 0 \tag{1}$$

$$\sum Y = 0 \tag{2}$$

$$\sum N = 0 \tag{3}$$

Forces and moments are broken down into the hydrodynamic components due to the hull (subscript h), the rudder (subscript r), and the propeller (subscript p); and the aerodynamic components due to the topsides (subscript t) and the wingsails (subscript w):

$$X_h + X_r + X_t + X_w = -X_p \tag{4}$$

$$Y_h + Y_r + Y_t + Y_w = 0 \tag{5}$$

$$N_h + N_r + N_t + N_w = 0 \tag{6}$$

For a given geometry, wind speed (TWS) and direction (TWA), and ship speed (V), the aerodynamic forces can be computed for any wingsail trim and the equations of motion allow the required propeller thrust (X_p) to be computed. In particular, firstly the leeway angle ϕ is computed solving the sway (5) and yaw (6) equations, which are coupled through the rudder angle (α_r), then the propeller thrust is computed solving the surge equation (4). The leeway angle must be solved iteratively starting from a guessed solution and in this paper the Nelder-Mead simplex method (Lagarias et al., 1998)

was used, while alternative approaches are described, for instance, in Larsson (1990) and Claughton et al. (2006).

This procedure can be repeated for each wingsail trim and therefore an optimisation function can be employed in order to find the trim giving minimum X_p. An off-the-shelf genetic algorithm implemented in Matlab, namely ga (Mathworks, 2010), was used to minimise X_p. The optimised parameters are the angle of attack of the fore (α_w) and aft (φ_w) airfoil on the lowest wingsail section, and the twist angle (τ_w) between the lowest and highest section. The program flowchart is shown in Figs 5 and 6.
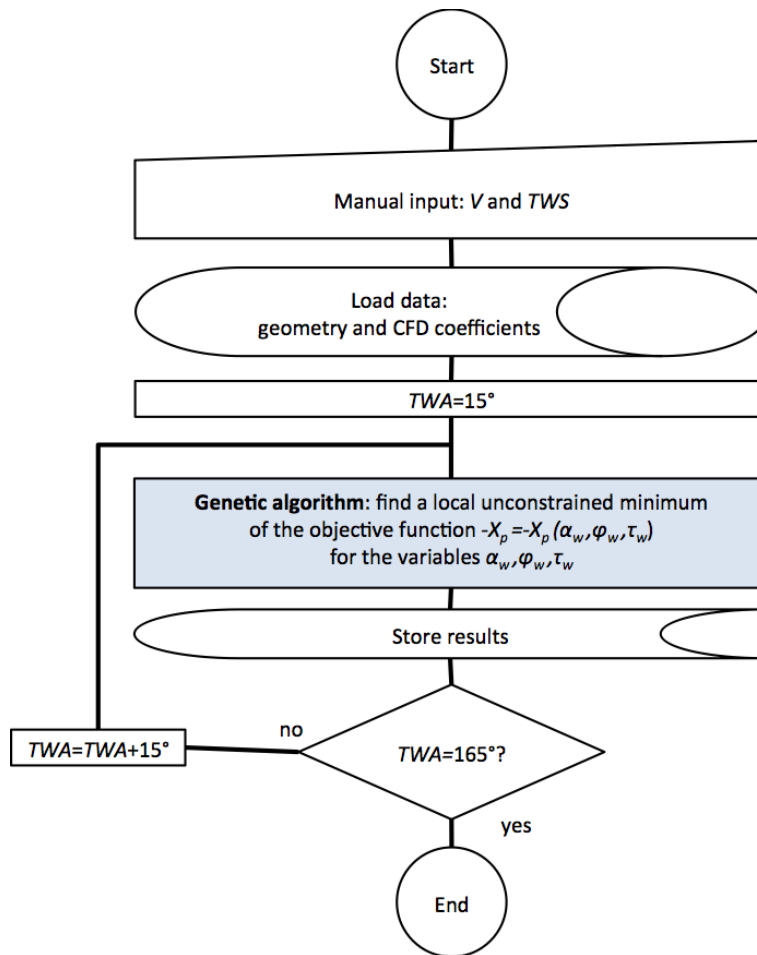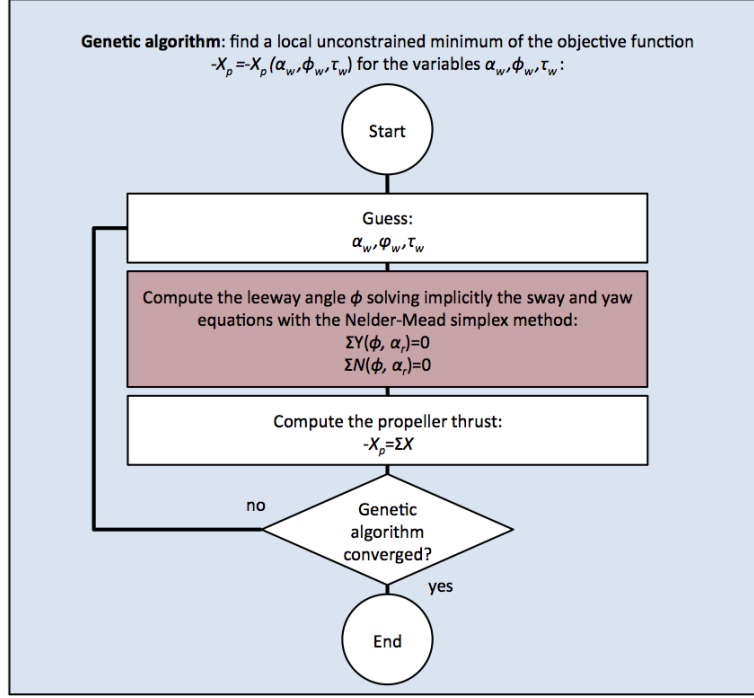
Figure 5: Program flowchart.

Figure 6: Program flowchart, detail of the genetic algorithm block.

2.3. Hull Model

The forces and moments due to the hull were modelled by adapting a typical approach used in manoeuvrability (Kijima et al., 1990) based on non-dimensional coefficients, which are denoted with a prime symbol in the following.

$$X_h = (\frac{1}{2}\rho_w V^2 L_{pp}d)X_h^{'} \tag{7}$$

$$Y_h = (\frac{1}{2}\rho_w V^2 L_{pp}d)Y_h^{'} \tag{8}$$

$$N_h = (\frac{1}{2}\rho_w V^2 L_{pp}^2 d)N_h^{'} \tag{9}$$

where ρ_w is the water density and V is the ship velocity.

Those coefficients are computed from Eqs. 10-21.

$$X'_h = X'_{uu} u'^2 + X'_{vv} v'^2 + X'_{vvvv} v'^4 \tag{10}$$

$$Y'_h = Y'_v v' + Y'_{vv} v' |v'| \tag{11}$$

$$N'_h = N'_v v' + N'_{vv} v' |v'| \tag{12}$$

$$X'_{uu} = -\frac{S_{wet}}{L_{PP} d} C_t \tag{13}$$

$$X'_{vv} = \frac{0.4B}{L_{PP}} - 0.006 \frac{L_{PP}}{d} \tag{14}$$

$$X'_{vvvv} = \frac{4B}{L_{PP}} - 0.002 \frac{L_{PP}}{d} \tag{15}$$

$$Y'_v = -\left(\frac{\pi}{2}\lambda + 1.4 C_b \frac{B}{L_{PP}}\right) \left[\left(25 C_b \frac{B}{L_{PP}} - 2.25\right)\tau + 1\right] \tag{16}$$

$$Y'_{vv} = \left[-2.5\left(1 - C_b\right)\frac{B}{d - 0.5}\right]\left[1 - \left(35.7 C_b \frac{B}{L_{PP}} - 2.5\right)\tau\right] \tag{17}$$

$$N'_v = -\lambda(1 - \tau) \tag{18}$$

$$N'_{vv} = \left(0.961(1 - C_b)\frac{d}{B} - 0.066\right)\left[1 + \left(58(1 - C_b)\frac{d}{B} - 5\right)\tau\right] \tag{19}$$

$$\lambda = \frac{2d}{L_{PP}} \tag{20}$$

$$\tau = \frac{d_a - d_f}{d} \tag{21}$$

where u and v are the ship velocity components in the longitudinal and transverse directions, and d_a and d_f are the aft and forward drafts, which were assumed to be equal in the present computation.

2.4. Rudder Model

Using a similar approach to the hull model, the forces and moments due to the rudder were computed from Eqs. 22-24.

$$X_R = -(1 - t_R)F_N \sin(\alpha_R) \tag{22}$$

$$Y_R = -(1 + a_H)F_N \cos(\alpha_R) \tag{23}$$

$$N_R = -(x_R + a_H x_H)F_N \cos(\alpha_R) \tag{24}$$

where

$$(1 - t_R) = 0.7382 - 0.0539C_b + 0.1755C_b^2 \tag{25}$$

$$a_H = 0.6784 - 1.3373C_b + 1.8891C_b^2 \tag{26}$$

$$x_R = -0.5L_{pp} \tag{27}$$

$$x_H = -(0.4 + 0.1C_b)L_{pp} \tag{28}$$

2.5. Wind Triangle

In order to compute the aerodynamic forces, the apparent wind experienced by the ship must be computed as a vectorial sum of the true wind and wind due to the ship speed $(-V)$. The apparent wind speed (AWS) and direction (AWA) vary with the height because of the true wind speed (TWS) increases with the height (Fig. 7). Assuming a logarithmic atmospheric boundary layer, the TWS was computed from Eq. 29.

$$TWS = \frac{u^*}{k} \log\left(\frac{z}{z_0}\right) \tag{29}$$

where u^* is the shear velocity which is computed by solving Eq. 29 for a given true wind speed at z=10 m; while z_0 is the water roughness height, which is computed with Eq. 30 as suggested by Cook (1985).

$$z_0 = 5 \cdot 10^{-5} \frac{(TWS|_{10})^2}{g} \tag{30}$$

where $TWS|_{10}$ is the true wind speed at z=10 m, and g=9.81 m/s^2 is the gravity acceleration.

At each horizontal section along the height, the apparent wind was computed using Eqs. 31-32. It should be noted that the leeway does not appear

in these equations because the true and apparent wind angles are defined with respect to the sailed course and not to the ship heading.

$$AWS = \sqrt{V^2 + TWS^2 + 2\,V\,TWS\cos(TWA)} \tag{31}$$

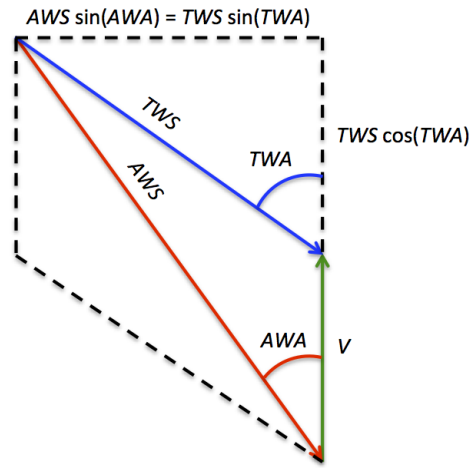$$AWA = \arctan\left(\frac{TWS\sin(TWA)}{V + TWS\cos(TWA)}\right) \tag{32}$$

Figure 7: True and apparent winds.

2.6. Topsides Model

The forces due to the wind on the topsides of the ship were computed with Reynolds-averaged Navier-Stokes (RANS) simulations where the topsides was modelled without the wingsails. A prismatic computational domain was used (Fig. 8). Lateral boundary conditions were located one L_{PP} from the ship; A Dirichlet condition was used on the two upwind faces and Neumann conditions were used on the two downwind faces. The bottom face was placed at the sea level and a no-slip condition was used, therefore the atmospheric boundary layer on the sea surface was modelled. The top face was placed half ship length from the bottom one and a symmetry condition was used. No-slip condition was used also on the topsides. A 1.7-million-cell non-structured grid of tetrahedral elements was used with ten prismatic layers on the non-slip boundaries in order to capture the boundary layers with

anisotropic cells. The steady incompressible RANS equations were solved and a k-ω SST turbulence model with wall functions was used. Simulations were performed with the code STAR-CCM+. Eleven simulations were performed for TWA ranging from 15° to 165° every 15°, where the inlet apparent wind profiles were computed for $V = 10$ knots (5.14 m/s) and $TWS|_{10} = 10$ knots. The aerodynamic forces X_t and Y_t so computed are shown in Fig. 9.

In order to compute the aerodynamic forces and moments on the topsides for a different AWS, these were scaled with the square of the AWS as, for instance for X_t in Eq. 33. It should be noted that scaling forces and moments from those measured for a given V and TWS leads to a small error as long as the ratio between V and TWS shows small variations.

$$X_t = X_t|_{10} \left(\frac{AWS}{5.14} \right)^2 \tag{33}$$

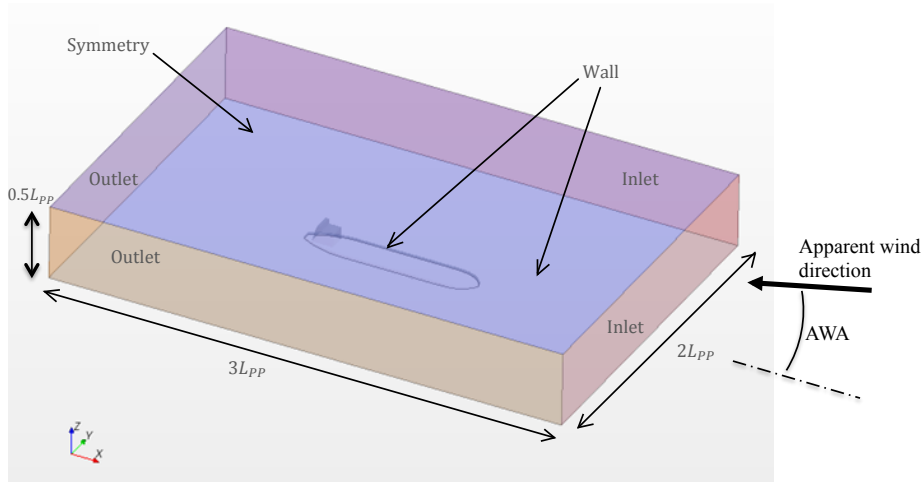where $X_t|_{10}$ is X_t computed at $AWS = 10$ knots.

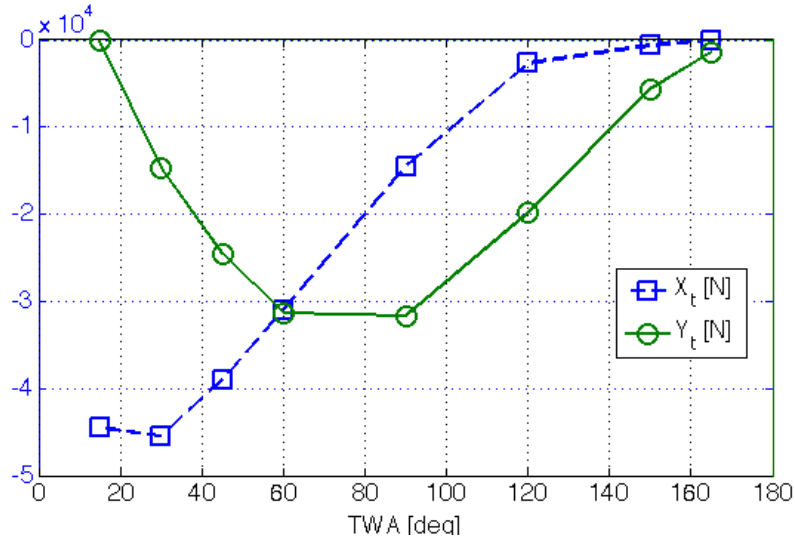Figure 8: Computational domain for the topsides model.

Figure 9: Aerodynamic forces on the ship topsides for different true wind angles.

2.7. Wingsail Model

2.7.1. Horizontal Sections

The optimum wingsail trim is not the one that maximises the thrust because the associated large side force which increases the hydrodynamic resistance. Assuming that the ship sails at a constant cruising speed, an increase of the hydrodynamic resistance must be balanced by an increase of propeller thrust. On the contrary, a lower wingsail thrust could lead to lower resistance and therefore might require lower propeller thrust. Therefore the wingsail trim must be optimised for the minimum propeller thrust required to sail at the chosen cruising speed.

In order to model the forces and moments generated by wingsails with different trims and planforms, firstly the forces and moments generated by bi-dimensional sections for different trims were computed with RANS and then these were integrated in the span-wise direction based on the chosen planform; where a correction was made in order to take into account of the non-infinite aspect ration of the wingsail. When sailing at large TWA, the drag generated by the wingsail contributes positively to the wingsail thrust; therefore also stalled conditions were investigated.

A square domain was used with the foils in the centre of the domain. The edges of the square were ten times the chord length of the fore foil. A Dirichlet

17

condition was used on the two windward edges and a Neumann condition on the two leeward edges. A no-slip condition was used on the foils and the grid resolution allowed solving the boundary layer without need of wall functions ($y+ < 1$). Figure 3 shows the hexahedral cells near the foils. The steady and unsteady incompressible RANS equations were solved for $TWA < 90°$ and $TWA > 90°$, respectively, with the k-ω SST turbulence model. The Reynolds number based on the total wing chord was $2.5 \cdot 10^6$. Simulations were performed with the code Fluent. Thirty-two angles of attack from $AWA_w = 0°$ to $AWA_w = 90°$ and five flap angles from $\varphi_w = 0°$ to $\varphi_w = 11°$ were tested, resulting in $32 \times 5 = 160$ simulations in total. As an example, Fig. 10 shows of the lift and drag coefficients based on the sum of the two chord lengths for different AWA_w and $\varphi_w = 5°$. The error bars show the numerical uncertainty at 95% confidence level due to the grid and time resolution that was estimated using the guidelines for uncertainty quantification in Viola et al. (2013).
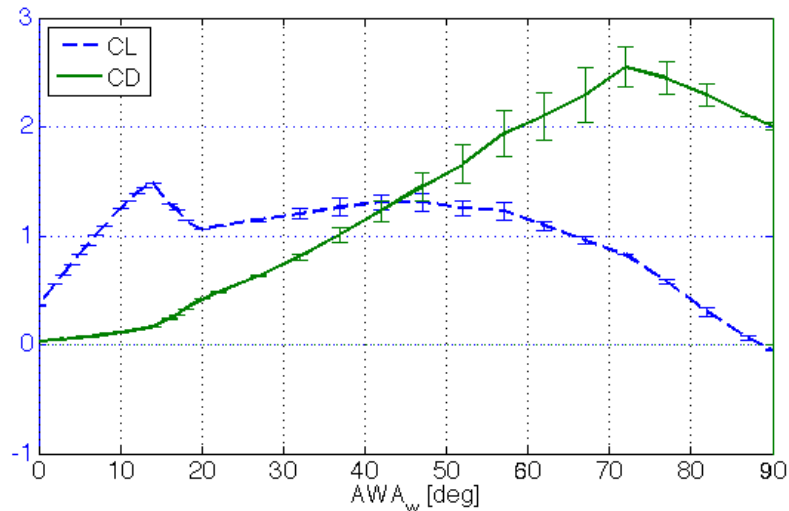

Figure 10: Lift and drag coefficients of a 2D section of the wingsail for a flap angle of 5°.

The data computed with these simulations were used to compute the lift and drag coefficients of each sail section of the wing where, for every height, the wingsail apparent wind speed ($AWS_w(z)$) and the apparent wind angle ($AWA_w(z)$) were computed with Eqs. 34 and 35, respectively.

18

$$AWS_w(z) = AWS(z) + \delta\sigma_t(z) \tag{34}$$

$$AWA_w(z) = AWA(z) + \delta\alpha_t(z) - \left(\alpha_w + \tau_w\frac{z}{h_w}\right) \tag{35}$$

where $AWS(z)$ and $AWA(z)$ are computed from Eq. 31 and 32, respectively; $\delta\sigma_t(z)$ and $\delta\alpha_t(z)$ are the local change in wind speed and direction, respectively, due to the presence of the topsides and are computed from the RANS simulations presented in Sec. 2.6 as a difference from the local velocity and the far field velocity at the same height; α_w is the wingsail angle defined as the supplementary angle between the chord of the lowest section of the wingsail and the ship velocity; and τ_w is the wing twist defined as the difference between the top and bottom section chords.

2.7.2. Spanwise Integration

The thrust and side forces due to the wings were computed from the rotation of the wingsail lift (L_w) and drag (D_w) forces computed with respect to the true wind direction. These were computed by spanwise integration of the lift and drag forces on the horizontal sections of the wing, where the lift force (Eq. 36) is corrected to take into account the limited aspect ratio (AR) of the wing and the induced drag force was added to the integrated drag force (Eq. 37).

$$L_w = \frac{\frac{1}{2}\rho_a \int\limits_0^{h_w} CL(z)\,c(z)\,[AWS_w(z)]^2\,\mathrm{d}z}{1 + \frac{2}{AR}} \tag{36}$$

$$D_w = \frac{1}{2}\rho_a \int\limits_0^{h_w} CD(z)\,c(z)\,[AWS_w(z)]^2\,\mathrm{d}z + \left(\frac{1}{\pi AR}\frac{L^2}{\frac{1}{2}\rho\int\limits_0^{h_w} c(z)\,[AWS_w(z)]^2\,\mathrm{d}z}\right) \tag{37}$$

where ρ_a is the air density; h_w is the height of the wingsail; $CL(z)$ and $CD(z)$ were interpolated from those computed in Sec. 2.7.1; $AWS_w(z)$ is computed with Eq. 34; $c(z)$ is the chord of the wingsail section; and $AWS_w(z)$ is computed with Eq. 35.

The yaw moment due to the wing was computed as the product of the side force and the geometric centre of the wingsail.

3. Results

The VPP was used to estimate the wingsail energy efficiency: the VPP was run in different conditions both with and without wingsails, then the ratio between the propeller thrust with wingsails (X_p) and without wingsails ($X_{p_{Base}}$) was computed. This ratio was computed for a range of TWA from $15°$ to $165°$. A ship with five wingsails sailing at 10 knots of speed with 10 knots of wind at 10 m height from the sea level was chosen as reference configuration, where each wingsail was 26.5 m height (similarly to the ship superstructures) and had a sail area of 578 m². A schematic diagram of the reference ship configuration is shown at the top of Fig. 11.

3.1. Wind Speeds

Figure 11 (left) shows the thrust ratio for true wind speeds from 7 knots to 13 knots. The three curves show that the wingsails do not allow much saving when sailing against the wind (i.e. low TWA), while the contribution is a maximum when sailing cross wind (i.e. $TWA = 90°$). In fact the wingsails have high lift/drag ratio and, at $TWA = 90°$, the ship direction is aligned with the lift. At slightly lower angles, the ship speed contributes positively to the apparent wind speed leading to a further little increase in the lift, which indeed increases with the square of the AWS. At even lower TWA, the lift contribution to the thrust decreases, while the drag projection along the ship course increases, leading to a lower overall wingsail propulsion. On the contrary, at $TWA > 90°$, the ship course becomes aligned with the drag. The drag is much smaller than the lift and therefore the wingsail thrust contribution decreases for TWA from $90°$ to $165°$. However, in strong breeze ($TWS = 13$ knots), the drag can be significant if the wingsails are stalled.

When the ship sails cross wind, the wingsails can allow a propeller thrust reduction of about 6%. Interestingly, a change of the wind speed of only ± 3 knots leads to almost double or half the propeller thrust reduction.

3.2. Ship Speeds

A similar trend effect is shown on the right of Figure 11, where three ship speeds are tested for a constant reference wind speed of 10 knots. Decreasing the ship speed by two knots allows an almost doubling the oil saving, and vice versa if the ship speed is increased by two knots. The oil saving is maximum in cross wind conditions and it increases if the wind speed increases and the ship cruising speed decreases. It can be concluded that decreasing the

cruising speed is a very efficient way to decrease the fuel consumption because it allows decreasing significantly the ship resistance and it also increases the wingsail contribution to the thrust.
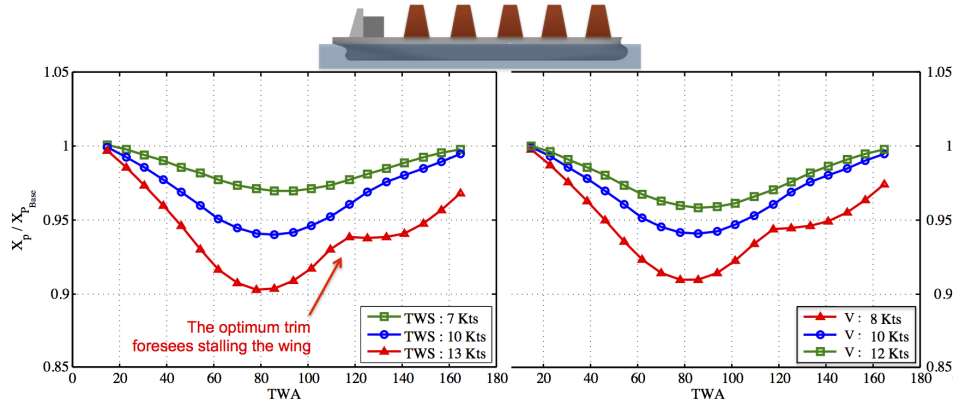

Figure 11: Propeller thrust ratio (with wingsails / without wingsails) for different true wind speeds (left) and ship speeds (right) versus the true wind angle.

3.3. Wingsail Area

Figure 12 shows how the thrust ratio varies for different wingsail sizes. In particular, the five reference wingsails have a total wingsail area ($S_w = 5$ x 578 m^2) of about 50% of the reference area (S_{ref}), which was chosen arbitrarily and which is shown by the green rectangle in the schematic drawing in Fig. 12. The total wingsail area was varied by modifying the wingsail chords, in order to achieve a total sail area which was 30% and 70% of the reference area. The three curves show that the higher the sail area the higher the oil saving. However, increasing the wingsail area from 50% to 70% of the reference area leads to a marginal gain in the oil saving from about 6% to 8%. The limited gain is due to the the loss of aerodynamic efficiency, in fact as is shown in the next section, a high wingsail aspect ratio is critical to achieve good performance.
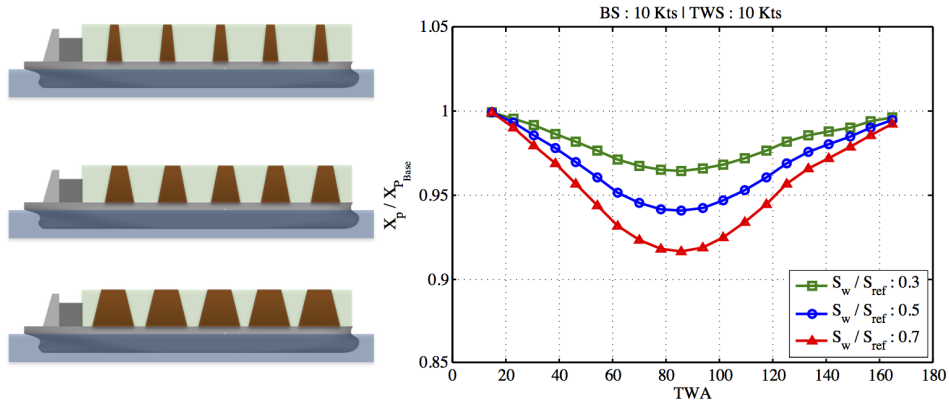
21

Figure 12: Thrust ratio for different wingsail areas versus the true wind angle.

3.4. Wingsail Aspect Ratio

What seems to significantly increase the oil saving is increasing the wing-sail aspect ratio, for instance dividing the total sail area between more wings. In Fig. 13, the total sail area and the height of the wingsails are constant but the number of wingsails and their chords vary. Distributing the total sail area between fewer low aspect-ratio wings, is shown to be significantly less efficient than adopting more high aspect-ratio wings. It must be noted that the results presented do not take into account the interactions between wingsails. However, as shown, for instance, by Ouchi et al. (2013), the wingsails interaction leads to enhanced aerodynamic efficiency. Therefore the benefit of more and closer wingsails compared to less and more separated wingsails is indeed expected to be even greater than presented in Fig. 13.
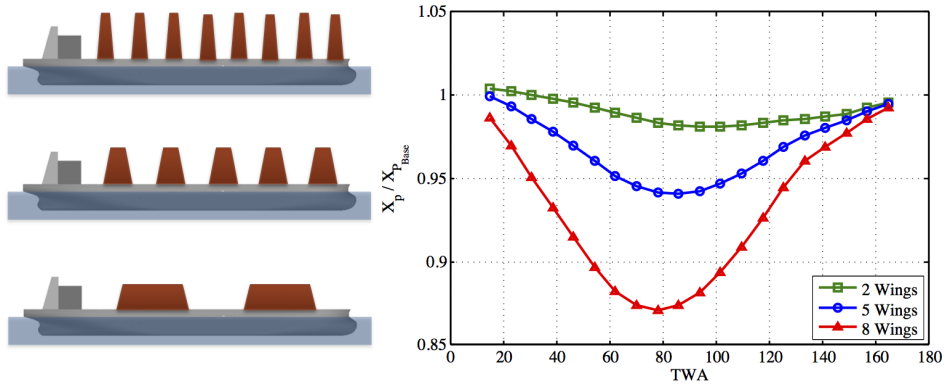
Figure 13: Thrust ratio for different wingsail aspect ratios for a fixed total wing area versus the true wind angle.

4. Conclusions

A Velocity Prediction Program for ships with propulsion assisted by wingsails was developed. The paper presents an original implementation where formulations originally developed for manoeuvrability are adapted to model the hydrodynamic forces and moments, while computational fluid dynamic simulations are used to model the aerodynamic forces and moments. Three parameters defining the wingsail trim and the rudder angle are optimised with a genetic algorithm in order to minimise the propeller thrust at a given ship speed, where the sway and yaw equations are used to compute the leeway and rudder angle, respectively.

The effect of key design parameters on the potential propeller thrust reduction is investigated in order to identify the configuration and the optimum operational conditions of a possible efficient windship. The ratio between the propeller thrust of a ship with and without wings is used as a measure of the energy efficiency. The effects of the wind speed and direction, of the ship speed, of the aspect ratio and of the total area of the wingsails are considered. It is shown that the maximum gain is reached when the ship sails across the wind. In particular, the wingsails allow a maximum propeller thrust reduction of about 10% when the ship sails at 10 knots in 13 knots of wind, or if she sails at 8 knots in 10 knots of wind. Decreasing the ship speed is found to be very beneficial because it allows the ship resistance to decrease and the contribution of the wingsails to the thrust to increase. The propeller thrust

reduction was found to be particularly sensitive to the wingsail aspect ratio, suggesting that an efficient wingsail should employ several tall wingsails rather than fewer shorter and larger wingsails.

5. Acknowledgements

6. References

Altosole, M., Figari, M., Martelli, M., Passano, L., Rocca, M., Giuliano, M., Piva, L., Oct 2014. Simulation study on the interaction between sailing and motor propulsion to optimize performance and control of the tall ship "amerigo vespucci". In: 15th International Congress of the International Maritime Association of the Mediterranean, IMAM 2013, Developments in Maritime Transportation and Exploitation of Sea Resources, A Coruna, Spain.

B9 Energy website, visited July 2011. www.b9energy.com.

Claughton, A. R., Wellicome, J. F., Shenoi, R., 2006. Sailing yacht design: Theory. University of Southampton, Computing Service.

Competitors of the America's Cup, 22 Feb 2012. AC72 Class Rule Version 1.1.

Cook, N. J., 1985. The designer's guide to wind loading of building structures. Building Research Establishment Report, Butterworths.

Cross, M., 19 June 1986. New generation clipper sails from Southampton. Vol. 1513-110 of 42. New Science.

Fujiwara, T., Hirata, K., Ueno, M., Nimura, T., May 2003. On aerodynamic characteristics of a hybrid-sail with square soft sail. In: The 13th International Offshore and Polar Engineering Conference, Honolulu, Hawaii, USA. pp. 326–333.

Holtrop, J., Mennen, G., July 1982. An approximate power prediction method. In: International Shipbuilding Progress. Vol. 335, 29. pp. 166–170.

International Maritime Organisation, 2009. Second IMO GHG Study 2009. CPI Books.

Kerwin, J., 1978. A Velocity Prediction Program for Ocean Racing Yachts revised to February 1978. Tech. Rep. 78-11, MIT, (part of the H. Irving Pratt Ocean Race Handicapping Project).

Kijima, K., Nakiri, Y., Katsuno, T., Furukawa, Y., 1990. On the manoeuvring performance of a ship with the parameter of loading condition. Journal of the Society of Naval Architects of Japan 168, 141–148.

Lagarias, J. C., Reeds, J. A., Wright, M. H., Wright, P. E., 1998. Convergence properties of the nelder-mead simplex method in low dimensions. SIAM Journal of Optimization 9 (1), 112–147.

Larsson, L., 1990. Scientific methods in yacht design. Annual Review of Fluid Mechanics 22 (1), 349–385.

Lemper, B., 2011. Shipping statistics and market review. No. 55. Institute of Shipping Economics and Logistics.

Mathworks, Sep 2010. Matlab mathematics r2010b.

National Maritime Research Institute of Japan website, visited in March 2014. www.nmri.go.jp.

Ouchi, K., Uzawa, K., Kanai, A., Katori, M., May 2013. Wind challenger the next generation hybrid sailing vessel. In: Third International Symposium on Marine Propulsors, SMP'13, Launceston, Tasmania, Australia. pp. 562–567.

Rosander, M., Block, O., 2000. Modern windships. Tech. rep., Pelmatic Knud E. Hansen.

Sacher, M., 2013. Aerodynamic study of AC72 wingsail. Master's thesis, Ecole Superieure des Techniques Aeronautique et de Construction Automobile.

Satchwell, C., 1985. Windship technology: proceedings of the International Symposium on Windship Technology, Windtech '85, Southampton, UK, April 24-25, 1985, Part 1. Elsevier.

Skysail website, visited July 2011. www.skysails.info.

United Nations Statistics Division website, visited Sep 2011. mdgs.un.org.

Viola, I. M., Bot, P., Riotte, M., 2013. Upwind sail aerodynamics: A RANS numerical investigation validated with wind tunnel pressure measurements. International Journal of Heat and Fluid Flow 39, 90–101.